metals

MDPI

Review

Degradation and Corrosion Challenges of the Nickel–Iron Catalysis for Oxygen Evolution Reaction: A Review

Branimir N. Grgur * and Aleksandra S. Popović

Department of Physical Chemistry and Electrochemistry, Faculty of Technology and Metallurgy, University of Belgrade, Karnegijeva 4, 11020 Belgrade, Serbia; apopovic@tmf.bg.ac.rs
* Correspondence: bngrgur@tmf.bg.ac.rs

Abstract

Green hydrogen production via water electrolysis is a cornerstone of the sustainable energy transition. However, the oxygen evolution reaction (OER) remains the kinetic bottleneck, limiting overall efficiency. Nickel–iron (NiFe)-based catalysts are among the most promising nonprecious materials for the OER in alkaline media, offering high activity and low cost. Nevertheless, their practical application at industrially relevant current densities (>100 mA cm^{-2}) is hindered by several challenges: structural degradation, uncontrolled surface reconstruction, metal dissolution (corrosion), particularly Fe leaching, and the ambiguous role of the fundamental mechanisms. This review critically discusses the current understanding of these degradation pathways, the influence of preparation methods, the interplay between Ni and Fe redox chemistry, and strategies for enhancing long-term stability. Future directions for designing durable NiFe OER electrocatalysts are also outlined. The paper also considers a strategy for investigating new catalysts using electrochemical and non-electrochemical techniques, devoted to young scientists interested in this field. In the Outlook and Perspective section, the key drawback is presented, and a possible strategy for improvement is discussed.

Keywords: hydrogen; electrocatalysis; electrolysis; stability

1. Introduction

Global primary energy consumption is projected to rise by more than 25% by the year 2040 [1]. Unfortunately, fossil fuels continue to supply the majority of this energy. According to the World Meteorological Organization (WMO), total carbon dioxide equivalent ($CO_{2,eq}$) emissions reached approximately 42 gigatons (Gt) in 2024 [2]. This includes 37.4 Gt from fossil fuel burning, with the rest mainly originating from land use vicissitudes, such as deforestation, contributing to a 2.0% increase over the previous record in 2023. These tendencies emphasize the pressing need to transition to scalable and environmentally friendly renewable energy transditions. In this context, green hydrogen (H_2) has gained attention as a favorable choice for considerably lowering the carbon footprint of global energy systems. Due to hydrogen high gravimetric energy density (hydrogen boasts the highest gravimetric energy density of all chemical fuels, delivering about 120 MJ kg^{-1}, approximately 33.6 kWh kg^{-1}, which is roughly 2.5 to 3 times greater than traditional fossil fuels like gasoline), wide availability, diverse applications, and near-zero carbon emissions potential, hydrogen is poised to play a key role in advancing a sustainable energy future [3]. However, current hydrogen manufacture remains heavily reliant on methods such as coal gasification and steam reforming of natural gas processes that generate considerable

Academic Editor: Leonid M. Kustov

Received: 7 June 2026
Revised: 1 July 2026
Accepted: 2 July 2026
Published: 6 July 2026

CO_2 emissions [4]. For instance, steam methane reforming proceeds via the following reaction [5]:

$$CH_4 + H_2O = 3H_2 + CO \quad (1)$$

And it is followed by the water–gas shift reaction:

$$CO + H_2O = H_2 + CO_2 \quad (2)$$

In that process, gray hydrogen is obtained, or if CO_2 is separated and stored, for example, underground via a very expensive route, blue hydrogen is obtained. A more feasible alternative is green hydrogen production by means of water electrolysis, where water is separated into hydrogen and oxygen using electricity sourced from renewables, mainly wind, solar, and hydroelectric power. Several technologies of water electrolysis exist that are in operation or under development, including the following: alkaline water electrolysis (AWE); proton exchange membrane electrolysis (PEME); solid oxide electrolysis cells (SOEC); and anion exchange membrane electrolysis (AEME) [6]. Each of these technological procedures has different industrial, productivity, and price characteristics. Unfortunately, all of these technologies have disadvantages. PEME is the most promising one. Proton conductors, usually perfluorosulfonic acid (PFSA) polymers, such as different Nafions, are widely used. They have acidity like ~1 M H_2SO_4; thus, due to corrosion, the noble metal catalyst (Pt, Ir, Pd, and their different alloys) must be used, which significantly increases their cost. Under relatively harsh conditions, high acidity, and an elevated temperature of 80-100 °C, the life span of membranes is only a few thousand hours. In addition, noble metal catalysts are very sensitive to impurities, like CO, H_2S, etc. SOEC works at elevated temperatures (typically between 600 °C and 900 °C), offering significantly higher energy efficiencies (often exceeding 90% in total system efficiency) compared to low-temperature alternatives, like PEME or alkaline electrolyzers. But the exotic ceramic and rare earth materials used for the electrodes and electrolytes are expensive to source and manufacture. Also, high operating temperatures provoke severe component degradation and slow start-up times. Anion exchange membrane (AEME) electrolysis is a relatively new promising green hydrogen technology but currently suffers from three primary disadvantages: poor membrane durability, low ionic conductivity, and high gas crossover risks [6,7]. Alkaline water electrolysis (AWE) is well established as a mature technology, the most conventional and widely adopted in industry. It sustains current attractiveness because of its low cost, using inexpensive non-conductive porous diaphragms; cathodes and anodes are typically constructed from low-cost, earth-abundant materials, like porous nickel, Raney nickel, or nickel-coated stainless steel meshes, and it is related to the other electrolysis technologies [7]. But the disadvantages of this technology are relatively high electrolysis voltage and high specific energy consumption, which arise from the oxygen evolution catalyst, which requires high overpotentials to sustain high current density [6,7]. Even so, green hydrogen produced through water electrolysis using renewable sources is a mainstay of low-carbon energy systems. It offers decarbonization of difficult-to-electrify sectors, such as steel and cement, mixing with natural or biogas, ammonia, and fertilizers, allowing for long-duration energy storage and providing seasonal and grid-balancing flexibility for large penetrations of variable renewables [8–11]. In addition, hydrogen-based internal combustion engines and hydrogen fuel cells are promising alternatives for transportation.

Therefore, this review paper aims to provide the state of the art of oxygen evolution catalysts for alkaline water electrolysis (AWE) and to critically consider the present status of the widely investigated Ni-Fe catalyst as the most promising in reducing electrolysis voltage, and, consequently, lowering specific energy consumption.

2. Fundamentals of OER and Water Electrolysis

As green hydrogen can be produced with a near-zero CO_2 lifecycle when produced with renewables, it is an important enabler of climate neutrality and decarbonized industrial value chains. Hence, to understand the different possibilities for leveraging oxygen overpotentials, the basis of water electrolysis is presented in this part. Among different types of water electrolyzers [12], even old technology, such as the alkaline electrolyzer (AWE), is still dominant due to its ease of maintenance, usage of inexpensive catalysts, low working temperatures, etc. [7]. The straightforward path to green hydrogen is electrochemical water splitting:

$$2H_2O \rightleftarrows O_2 + 2H_2 \tag{3}$$

But the oxygen evolution reaction (OER) in alkaline solution is the kinetic bottleneck. Usually, it involves the formation of strongly bound intermediates (like *OH, *O, *OOH), and four electron transfers are required:

$$4OH^- \rightleftarrows 2H_2O + O_2 + 4e^- \tag{4}$$

Thus, it is slow and energy-demanding [13].

Partial reactions for hydrogen (HER) and oxygen evolution (OER) reactions in alkaline solutions are:

$$2H_2O + 2e^- \rightleftarrows H_2 + 2OH^- \tag{5}$$

And

$$4OH^- \rightleftarrows O_2 + H_2O + 4e^- \tag{6}$$

The theoretical decomposition voltage, U_0, of water is 1.23 V. Due to different overpotentials, η, and resistance of the electrolyte and diaphragm, operating voltages are in the range of 1.7 to 3 V [14]. Theoretically, for 1 kg of H_2, it is necessary to use ~33.6 kWh of electric energy. In real systems, specific energy consumption, w_s, per kg of H_2 is much higher, in the range from 50 kWh to 70 kWh [14]. The specific energy consumption is given by:

$$w_s = \frac{UIt}{m(H_2)} = \frac{(U_0 + \eta_+ + \eta_-)It}{m(H_2)} = U \times k \tag{7}$$

where, under the same current, time, and mass of hydrogen, only the voltage can decrease specific energy consumption. Hereafter, lowering the electrolysis voltage at constant current, time, and mass of hydrogen, by finding good electrocatalysts that will decrease overpotentials, plays a crucial role.

To understand the catalytic role of the catalyst, it is necessary to see the structure of the electrolysis voltage:

$$U = U_0 + \eta_+ + |\eta_-| + I\sum_i R_i \tag{8}$$

where U_0 is the difference between anodic and cathodic reversible potentials and is defined as:

$$U_0 = E_t(O_2\,|\,OH^-) - E_r(H_2\,|\,H_2O) \tag{9}$$

Or, by taking into account the standard reversible potentials, ${E_r}^\theta$ for oxygen is 1.23 V, and for hydrogen, it is 0 V, neglecting the partial pressure. Then, the following is obtained:

$$U_0 = 1.23 - \frac{2.3RT}{4F}\log\left(\frac{1}{c^4(OH^-)}\right) - \left(0 - \frac{2.3RT}{2F}\log\left(\frac{1}{c^2(OH^-)}\right)\right) \tag{10}$$

Or after rearrangement:

$$U_0 = 1.23 - 0.0591 \times \mathrm{pH} + 0.0591 \times \mathrm{pH} = 1.23\ \mathrm{V} \tag{11}$$

Therefore, at a given temperature and concentration of OH^-, the reaction rate cannot be significantly improved with U_0. But the overpotentials are directly connected with current density and catalytic properties of the electrode materials. The current density depends on overpotentials, as given by

$$j_\pm = j_{0,\pm} \exp\left(\pm \frac{\alpha_\pm F \eta_\pm}{RT}\right) \tag{12}$$

where "+" is valid for anodic and "−" is valid for cathodic current density, where $\eta = E - E_\mathrm{r}$ and j_0 is the exchange current density, which contains exponential terms of E_r, and, most importantly, Gibbs energy $\Delta G^\#$ of activation, which is crucial for the increase rate of the reaction, and α is the transfer coefficient that is dependent on reaction mechanisms and can have values of 0.5, 1, 1.5, and 2. In Equation (12), the Tafel equations can be derived:

$$\eta = \pm \frac{2.3RT}{\alpha_\pm} \log\left(\frac{|j_\pm|}{j_{0,\pm}}\right) \tag{13}$$

From the pre-exponential terms, the Tafel slope can be derived:

$$b_\pm = \pm \frac{2.3RT}{\alpha_\pm F} \tag{14}$$

Taking into account the transfer coefficient, Tafel slopes can be 120, 60, 40, and 30 mV dec^{-1}. The importance of the Tafel slope, which is connected with the mechanism, can be seen in Figure 1a,b. Figure 1a shows the structure of the alkaline electrolyte electrolysis potentials for two different Tafel slopes (for simplicity, j_0 and b, for OER and HER, are taken with the same values). As can be seen, the voltage of the electrolysis at the constant current density is ~0.2 V lower for the Tafel slope of 60 mV dec^{-1} than for 120 mV dec^{-1}. This is mainly a consequence of the better catalytic properties of the catalysts. According to Equation (8), Figure 1 shows electrolysis voltages for two different Tafel slopes, and it is obvious that with lower Tafel slopes, water splitting is more energetically favorable, which directly decreases specific energy consumption and the price of hydrogen.

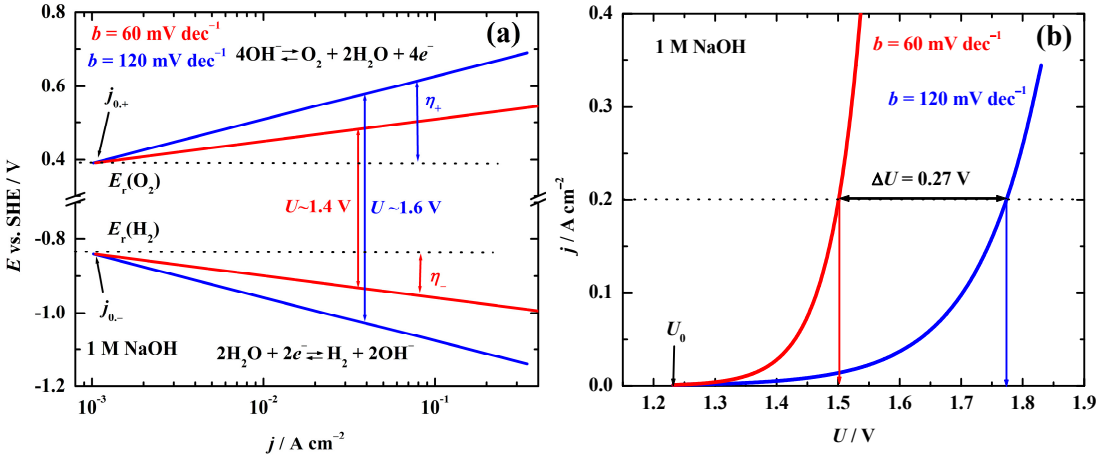

Figure 1. Simulated (**a**) structure of the potentials and (**b**) voltages of alkaline electrolyte electrolysis for two different Tafel slopes.

Considering OER, the four-electron transfer is highly demanding, which implies a very complex mechanism [15]. In the oxygen evolution reaction (OER), the classical Adsorbate Evolution Mechanism (AEM) and the lattice oxygen mechanism (LOM) differ in both the reaction pathway and the origin of the evolved oxygen [16–18]. In the AEM, the catalyst serves mainly as a surface for stepwise oxidation of adsorbed intermediates (*OH, *O, *OOH), and the produced O_2 comes entirely from water. In contrast, LOM involves direct participation of oxygen atoms from the catalyst lattice; an oxygen atom from the solid can leave the structure and combine into O_2, creating an oxygen vacancy that is later refilled by oxygen from water. Because of this, LOM can bypass some of the energetic limitations typical of the AEM and potentially enhance activity, although it may also compromise structural stability due to continuous lattice involvement. The mechanism of the AEM and LOM can be presented with the following kinetic sequences:

AEM

$$S + OH^- \rightarrow S\text{-}OH_{ads} + e^-$$

$$S\text{-}OH_{ads} + OH^- \rightarrow S\text{-}O^* + H_2O + e^-$$

$$S\text{-}O^* + OH^- \rightarrow S\text{-}OOH^* + e^-$$

$$S\text{-}OOH^* + OH^- \rightarrow S + O_2 + H_2O + e^-$$

LOM

$$M(II)\text{-}O_{lat}H + OH^- \rightarrow M(III)\text{-}O_{lat} + H_2O + e^-$$

$$M(III)\text{-}O_{lat} + \rightarrow M(IV)\text{-}O^{\bullet} + e^-$$

$$2[M(IV)\text{-}O^{\bullet}] \rightarrow M(II)\text{-}V_O + O_2(g)]$$

$$2M(II)\text{-}V_O + 2OH^- \rightarrow 2M(II)\text{-}O_{lat}H + 2e^-$$

For the AEM, in the reactions, only surface active centers, *S*, are involved, and metals do not change valence states, while for LOM, the lattice metal–oxide is involved.

Along with the AEM and LOM, recently, the oxide pathway mechanism (OPM) and the Mars–van Krevelen mechanism have been proposed as further alternative directions for O–O bond creation. OPM contains direct coupling of two adjacent metal–oxygen positions without lattice oxygen removal, but it involves exact metal–metal distances on the surface, which are problematic to reach and sustain under working conditions [19–21]. The Mars–van Krevelen mechanism, thoroughly connected to LOM, explicitly includes the exchange of lattice oxygen with the electrolyte; its main restriction is that the constant extraction of lattice oxygen can lead to catalyst dissolution if oxygen vacancies are not adequately refilled. Even though the direct O–O coupling for oxygen evolution is well known, the study of the OPM for OER is still in its recent stage. Compared to the AEM and LOM, there are additional unknown factors that may affect the OPM and Mars–van Krevelen pathway, and even the identification of the OPM remains an inspiring task [19]. Understanding the conditions under which each mechanism operates, and its particular limitations, is crucial for designing stable and active OER electrocatalysts [22]. Consequently, the improvement of OER characteristics is mainly connected with lowering the Tafel slopes, decreasing the Gibbs energy $\Delta G^{\#}$ of activation for adsorbed intermediates, and finding the catalyst prone to lattice attack.

After all, it is not surprising that Fabbri and Schmidt 2018 wrote that "Even though the splitting of water was known since the 19th century, after Paets van Troostwijk and Deiman, as well as Nicholson and Carlisle, discovered that (static) electricity can split the water into hydrogen and oxygen, the oxygen evolution reaction is still an enigma [23]."

The state of the art of the Ni-Fe catalyst, with synthesis methods and characteristics, is discussed in the following text.

3. The Catalyst Synthesis Methods and Their Influence on the Activity

The noble metals and their oxides (like IrO_2, RuO_2, Pt) are considered as the well-known catalysts for the oxygen evolution reaction but are limited by their price and shortage for scale-up. But, due to the difficulties with the adsorption of the oxygen intermediates in basic solutions, those catalysts show modest activity [24–27]. Therefore, due to modest activity and high price, noble metals and their oxides are not suitable for alkaline water electrolysis as an anode catalyst. On the contrary, iron group metals, Fe, Ni, and Co, are of intense research due to corrosion stability in alkaline electrolyte and their relatively low price. However, as shown by Si et al. [28], overpotentials at 10 mA cm^{-2}, for the metals covered with oxy-hydroxide, were obtained by cycling of the pure metals in the oxygen evolution region. For NiOOH, the overpotential is 441 mV; for CoOOH, it is 454 mV; and for FeOOH, it is up to 1.7 V vs. RHE, and it did not show any significant activity.

Afterward, the innovative work of Corrigan [29] revealed almost four decades ago that a thin-film nickel oxide electrode showed insignificant OER until overpotentials in excess of 400 mV were applied, and absorption of trace iron contamination (1 to 10 ppm) effectively lowered the overpotential and improved activity. Iron is precipitated into the NiOOH film when ferric nitrate is added to the nickel nitrate solution used for electrodeposition. Higher concentrations of iron precipitated into a complex iron–nickel hydrous oxide effectively catalyzed the OER by decreasing the Tafel slope from about 70 mV dec^{-1} with no iron existing to about 25 mV dec^{-1} with 10–50% of the iron. This result was later confirmed and extended by Trotochaud et al. [30], who methodically studied electrodeposited $Ni(OH)_2$ and NiOOH films in purified electrolyte. They showed unambiguously that Fe-free NiOOH required >400 mV to reach 10 mA cm^{-2}, although careless absorption of Fe sunk η_{10} by ~200 mV, emphasizing the significance of Fe in main activity. These low-activity starting points persist in significant control experiments, prompting the scientists to state that Ni alone cannot explain the outstanding activity that is often reported in the literature. Nickel–iron (oxy)hydroxides have become the standard benchmark for a non-noble OER electrocatalyst in alkaline electrolyte, but their development has been anything but straightforward.

The state-of-the-art, earth-abundant electrocatalysts for the OER in alkaline media, for now, are nickel–iron layered double hydroxides (NiFe LDHs). Initially, in 2013, Gong et al. [31] described ultrathin NiFe LDH nanoplates on carbon nanotubes with an overpotential of ~210 mV at 10 mA cm^{-2}, establishing their potential for OER. Additionally, dissimilar synthetic methods were developed toward activity improvement, morphology control, and stability. Due to different preparation methods and synthesis conditions, reported overpotentials for a current density of 10 mA cm^{-2} vary between 130 mV and 350 mV [32]. The most broadly used approaches are co-precipitation, hydrothermal synthesis, electrodeposition, and, moderately less used, urea-assisted hydrolysis, microwave-assisted synthesis, and the mechanochemical processes.

The structure of the LDH catalyst is highly intricate, as illustrated in Figure 2 [33]. Its general formula is $[M^{2+}{}_{1-x}M^{3+}{}_x(OH)_2]^{x+}[A^{n-}{}_{x/n}]^{x-}\cdot mH_2O$, where M^{2+} and M^{3+} represent divalent and trivalent metal ions, respectively. A^{n-} represents negatively charged interlayer guest anions (e.g., $CO_3{}^{2-}$, $NO_3{}^-$, Cl^-, $SO_4{}^{2-}$), and the molar ratio of M^{3+} to (M^{2+} + M^{3+}) is represented by x, which typically ranges from 0.2 to 0.33. The LDH structure is derived from brucite-like $Mg(OH)_2$ layers, which consist of infinite sheets of edge-sharing $M(OH)_6$ octahedra. In these octahedral, metal cations occupy the center, surrounded by six OH^- ions at the corners. The host layer acquires a positive charge due to the coexistence of divalent and trivalent metal cations, and this charge is balanced by anions along with water

molecules located in the interlayer region. The basal spacing (d) in LDH materials refers to the distance from the center of one host layer to the center of the adjacent layer; thus, it equals the sum of the brucite-like layer thickness and the interlayer space.

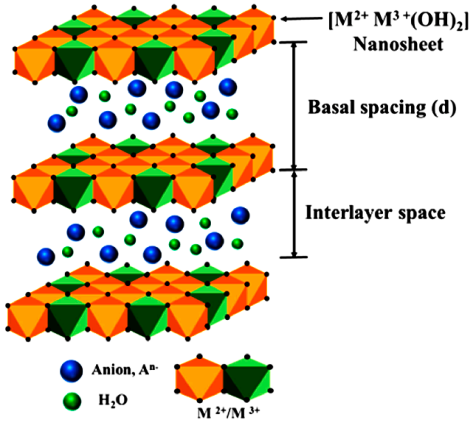

Figure 2. The structure of the LDH catalyst. Adapted from Ref. [33].

As the structure is very complex, the morphology significantly varies, like hexagonal platelets, nanosheets, nanolayers, microspheres, flakes, and nanoflowers, as can be seen in Figure 3 [34].

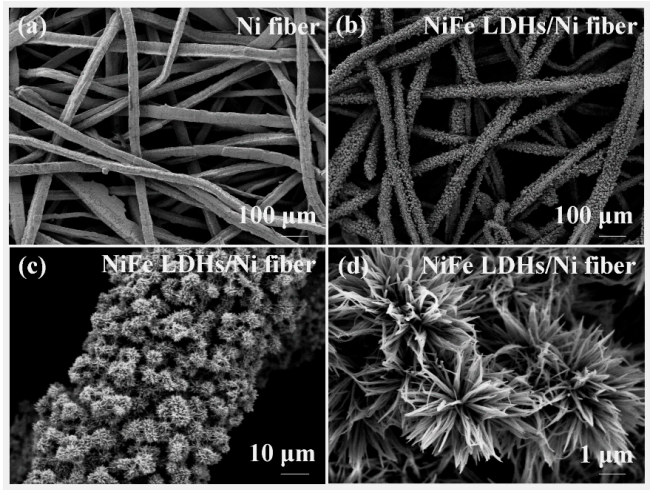

Figure 3. SEM images of Ni fiber electrode (**a**) and NiFe LDHs/Ni fiber electrode (**b**–**d**) under different magnifications. Adapted from Ref. [34].

Co-precipitation is a common method involving the precipitation of nickel and iron salts under alkaline conditions, which permits control of the composition but produces powders that usually exhibit low conductivity and rather modest performance at high currents (for example, ~360 mV at 10 mA cm^{-2}) [35]. Hydrothermal synthesis can grow NiFe LDH nanosheets straight onto a conductive substrate for an enhancement in electrical contact, alongside robustness at high currents. Li et al. [36] reported the hydrothermally grown NiFe LDH onto nickel foam (NF) that reached 175 mV at 10 mA cm^{-2} with constant operation at 500 mA cm^{-2} for 50 h. Liu et al. [37] investigated a simple one-step hydrothermal method and at a current density of 100 mA cm^{-2} and achieved an overpotential of 387 mV and acceptable stability after a constant operation of 28 h at 1.63 V vs. RHE (η = 400 mV) at a current density of ~25 mA cm^{-2}. Hydrothermal growth of NiFe LDH nanosheets on nickel foam and Raney Ni precursor is found to form vertically aligned electrodes with high surface area (>150 $m^2 \cdot g^{-1}$) and low overpotentials, ~124 to

300 mV at 10 mA·cm^{-2} and ~320 to 400 mV at 100 mA·cm^{-2} in 1 M KOH [38]. Guoqi et al. [39] investigated NiFe LDH synthesized by the hydrothermal method mixed with terephthalic acid (TPA) in 1 M KOH that displays good performance at the current density of 2 mA cm^{-2} at an overpotential of 270 mV, with a Tafel slope of 40 mV dec^{-1}. At higher current densities, 10 mA cm^{-2} and 100 mA cm^{-2}, overpotentials were 320 mV and 570 mV. Thermal decomposition (calcination) of the Ni/Fe composite is a scalable route for NiFe oxides; activity is then sensitive to calcination conditions, time, after-treatment, and Ni:Fe composition, with overpotentials at 100 mA·cm^{-2} being ~280–300 mV, depending on optimization [40].

Electrodeposition is one of the most widely used methods for the synthesis of the NiFe DLH. Quiroz et al. [41] investigated electrodeposited NiFe LDH using the electrolyte bath containing $Ni(NO_3)_2 \times 6H_2O$ and $Fe(NO_3)_3 \times 9H_2O$ as precursors of nickel and iron. The molar ratio of Ni:Fe in the electrolyte bath varied between 1:1, 2:1, 3:1, 4:1, 5:1, 10:1, 12:1, 15:1, and 20:1. The Ni:Fe electrodeposits of 15:1, corresponding to 9.83 at.% Ni, 28.07 at.% Fe, and 62.10 at% O, determined using EDS, show the best catalytic activity for OER, with the low Tafel slope of 38 mV dec^{-1} and overpotentials of 206 mV and 244 mV at 30 mA cm^{-2} and 100 mA cm^{-2} in 1 M NaOH. At the current density of 400 mA cm^{-2}, a constant overpotential of ~300 mV is achieved throughout 25 h. Electrodeposition of the NiFe/NF electrode shows high catalytic activity towards OER in alkaline solutions that only needs an overpotential of 200 mV to initiate the reaction, and overpotentials for current densities of 50 and 500 mA cm^{-2} reached 250 and 620 mV, respectively [42]. Swierk et al. [43] present a comprehensive manuscript about the OER activity of the electrodeposited NiFe LDH in 1 M KOH, varying Fe content from 0 to 100%. At overpotentials of 400 mV, they obtained current densities of: 0% Fe 2 mA cm^{-2}, 10% Fe 15 mA cm^{-2}, 24% Fe 35 mA cm^{-2}, 34% Fe 40 mA cm^{-2}, 75% Fe 10 mA cm^{-2}, and 100% Fe 5 mA cm^{-2}. At 10 mA cm^{-2}, determined overpotentials are: 0% Fe 540 mV, 10% Fe 375 mV, 24% Fe 345 mV, 34% Fe 330 mV, 75% Fe 400 mV, and 100% Fe 440 mV. The Tafel slopes for these electrodes are in the range from 60 to 65 mV dec^{-1}, except for pure nickel, with 105 mV dec^{-1}.

In urea-assisted hydrolysis, the growth of NiFe LDH is controlled by the sluggish decomposition of urea. Wu et al. investigated urea-assisted NiFe LDH and showed that interlayer anions and the morphology of NiFe LDH are tunable via urea hydrolysis, but the authors did not investigate OER [44]. Zuber et al. [45] investigated the urea-assisted synthesis of NiFe LDH from nitrate, sulfate, and mixed salt. Applying the current density of 10 mA cm^{-2}, overpotentials for nitrate are 425 mV, 460 mV for sulfate, and 346 mV for mixed precursor salt. Nevertheless, the permanence of the electrodes during the stability test was very low.

Microwave-assisted synthesis of NiFe produces thin nanosheets in a very short period of time, accordingly permitting the high surface area with low overpotentials, such as 250 mV at 10 mA cm^{-2}, as reported by Hou et al. [46]. Iwasaki et al. [47] investigated mechanochemical synthesis methods, but such methods produce low crystallinity of the product. Molina-Muriel et al. [48], using a mechanochemical process, investigated the obtained product for OER, and a current density of 10 mA·cm^{-2} achieved overpotentials of 220 mV and a Tafel slope of ~100 mV·dec^{-1}, demonstrating admirable OER kinetics. In addition, the catalyst verified robust permanence, keeping a potential of about 1.55 V (η = 520 mV) during 35 h at a current density of 100 mA·cm^{-2} and 1.75 V (η = 520 mV) at 1 A·cm^{-2}.

Beyond structural factors, the type and concentration of the electrolyte also play a critically important role. Del Rosario et al. [49] explore how hydroxide cations affect the OER. They demonstrate that the activity of IrO_x and $NiCo_2O_3$ increases in the order $Li^+ < Na^+ < Cs^+ < K^+$ in 1 M MOH solutions. This trend arises mainly from differences in the

interaction strengths of specifically adsorbed OH_{ad} intermediates and non-specifically adsorbed alkali metal cations (AM^{+}_{ad}) inside the electric double layer. Comparable results are reported by Garcia et al. [50] for nickel oxyhydroxide (NiOOH), with the cation effect following $Cs^+ > Na^+ > K^+ > Li^+$, confirming an intrinsic influence of the cation on OER activity. In 1 M KOH, K^+ ions favor better ionic movement and more uniform interfacial charge separation, which lowers overpotentials compared to 1 M NaOH, where strongly hydrated Na^+ ions hinder ion movement and block access to the active centers [51]. Park et al. [52] investigate the effect of NaOH concentration on IrO_2 anodes' activity. Applying a constant overpotential of 420 mV and increasing NaOH concentrations from 0.01 to 0.02, 0.10, 0.50, and 1.0 M yields the current densities of 3, 5, 40, 50, and 80 mA cm^{-2}, respectively. Increased NaOH concentration improves conductivity (reducing *IR* losses), which benefits kinetics and generally drops the overpotentials by about 200 mV under an applied current density of 100 mA cm^{-2} when comparing 1 M and 30% KOH [53]. Luo et al. [54] hydrothermally prepared a NiFe-LDH@Fe_2O_3@NF composite and observed a remarkable pH-dependent activity increase. At 1.50 V vs. RHE (η = 0.27 V), raising the pH from 13.30 to 14 boosts the current density from roughly 20 mA cm^{-2} to an impressive 250 mA cm^{-2}.

4. Stability Challenges and Degradation Mechanisms

The stability of the NiFe electrodes depends on several factors, including their morphology, adhesion to the substrate, degree of crystallinity, and electrical conductivity [55]. Therefore, both the synthesis method and the electrode design must be carefully tailored to ensure that the resulting materials maintain high activity and durability under operating conditions relevant to the oxygen evolution reaction (OER). The chosen synthesis pathway directly influences the structure and function of NiFe-based catalysts. Although NiFe catalysts perform excellently in laboratory settings, their application in industrial-scale alkaline electrolysis requires an optimal chemical composition, a large specific surface area, scalable production methods, and long-term durability to sustain low overpotentials at high current densities over extended operation [7,22]. Dissolution is typically the primary driver of catalyst performance degradation. During the oxygen evolution reaction (OER), harsh operating conditions, such as strongly acidic or alkaline media and oxidative environments, can readily trigger this process. The dissolution may also arise from surface reconstruction and lattice oxygen participation. This is typical for LOM, where the lattice metal oxides, such as M(II)–O_{lat}H, M(III)-O_{lat}, and M–O^{2-}(lattice), and a highly reactive oxygen radical, M(IV)-$O^{\bullet}$, are involved, and where metals (Ni, Fe) change their valence state, producing vacancies, such as M(II)–V_O. If the vacancies are not effectively converted to the lattice, degradation of the catalyst can occur. The rate-determining step (RDS) depends on the catalyst and cannot be simply determined. Even though the LOM is considered a favorable path, on some occasions, the oxygen lattice from the subsurface could be involved, which could produce material degradation (corrosion). When the lattice oxygen mechanism (LOM) operates, oxygen atoms are removed from the solid lattice, creating oxygen vacancies (M-V_O). An oxygen vacancy in a NiFe OER catalyst refers to a missing oxygen atom in the crystalline structure of nickel–iron oxides/hydroxides (like NiFe-LDH). This deliberate structural defect acts as a powerful tool to maximize water-splitting efficiency. The overall extraction can be described as:

$$2[\text{M(IV)-O}^{\bullet}] \rightarrow \text{M(II)-V}_O + O_2(g)] \quad (15)$$

Under steady-state conditions, vacancies can be repaired by hydroxide ions from the electrolyte:

$$\text{M–V}_O + OH^- \rightarrow \text{M–O}_{lat}\text{H} + e^- \quad (16)$$

At low overpotentials, the healing rate balances vacancy generation. However, at high current densities, the extraction rate exceeds the healing capacity. Insufficient replenishment leads to continuous vacancy accumulation, which ultimately induces lattice distortion. Consequently, V_O accumulates, leading to lattice distortion, loss of crystallinity, and structural collapse [56]. On the other hand, the AEM involves four concerted proton-coupled electron transfer steps on a single metal site, producing specific oxygen intermediates: *OH, *O, and *OOH. The Sabatier principle dictates that the adsorption energies of these intermediates are linked by a linear scaling relation. Because of this, it is practically impossible to independently optimize the binding strengths of both intermediates on a single site. This thermodynamic interdependence creates an unavoidable theoretical overpotential limit of approximately 0.37 V to 0.40 V. This overpotential hurdle prevents AEM catalysts from achieving the highly efficient reaction rates required for commercial electrolyzers. In addition, even Fe is the principal active site in the NiFe AEM cycle, optimizing the binding energy of the oxygen intermediates. However, under highly oxidative anodic potentials, these surface Fe species are prone to leaching into the electrolyte.

In practice, dissolution under oxidizing electrochemical conditions is highly complex. Studies indicate that dissolution pathways vary significantly, depending on factors such as crystal facets, support substrates, and applied potentials. Therefore, further investigation is needed to fully elucidate these intricate mechanisms. Beyond the intrinsic stability of the catalyst itself, dissolved species or leached ions in the electrolyte can also affect catalytic performance—and may even undergo redeposition during prolonged electrolysis [22]. Although this aspect has received comparatively less attention, it is believed to play a critical role in determining both activity and long-term stability. From the industrial perspective of wives, the operational temperature is crucial. Although practically all experiments are done at room temperature, there are missing investigations at elevated temperatures, e.g., ~80 °C. The temperature dependency of NiFe-based OER catalysts' activity is examined by Li et al. [57], who find that higher temperatures enhance mixed ionic conductivity and accelerate OER kinetics. This finding highlights the need to characterize catalysts under realistic operating temperatures. On the other hand, Pascuzzi et al. [58] concluded that while NiFe (oxy)hydroxide is a highly active alkaline OER electrocatalyst, its stability is strongly tied to operating conditions. Under mild conditions (25 °C, 1 M KOH), only minor structural and compositional changes occur. However, at higher temperatures (75 °C) and more realistic alkali concentrations (5–10 M KOH), iron dissolution speeds up, lowering the Fe/Ni percentage and growing charge transfer resistance, which speeds up OER activity. NiFe layered double hydroxide (LDH) is widely considered as one of the most active, non-noble metal electrocatalysts for the OER in alkaline water electrolysis. While highly effective at the lab scale, large-scale industrial application faces specific synthetic hurdles and operational bottlenecks. Scaling up NiFe LDH production requires moving away from tedious, small-batch lab procedures to rapid, high-yield, and cost-effective methods. NiFe LDH is essentially a semiconductor. At industrial-scale current densities (>500 mA cm^{-2}), high electrical resistance causes severe Ohmic heating and energy losses. Also, at high current densities, gas bubbles can become trapped in the catalyst's porous structures. This gas blanketing blocks active catalytic sites and limits electrolyte penetration, significantly increasing overpotentials and decreasing overall energy efficiency. The aggressive bubbling subjects the catalyst layer to mechanical stress, often causing the NiFe film to peel or delaminate from the conductive substrate (e.g., nickel foam).

In addition to parameters such as configuration, morphology, and actual surface area, the catalytic activity of NiFe oxides or oxyhydroxides in the OER is strongly affected by the oxidation states of nickel and iron. Specifically, the splitting of 3d orbitals into lower-energy t_{2g} and higher-energy e_g levels plays a key role. Ni^{2+} (t_{2g}^6, e_g^2) typically exhibits low

activity; however, its oxidation to Ni^{3+} (t_{2g}^6, e_g^1) results in an e_g occupancy close to one, which optimizes metal–oxygen covalency and the energies of reaction intermediates adsorption, thereby enhancing catalytic behavior [30,59]. Further oxidation to Ni^{4+} (t_{2g}^6, e_g^0) strengthens metal–oxygen bonds, which can increase activity but often reduces durability [58,59]. The iron, in the configuration Fe^{2+} (t_{2g}^4, e_g^2), leads to extra e_g electrons that generally weaken activity due to stronger antibonding interactions. Nevertheless, mixed Fe^{2+}/Fe^{3+} valence states can increase charge transport inside the crystal framework [29]. On the contrary, Fe^{3+} (t_{2g}^3, e_g^2), with its half-filled e_g orbitals, enhances the activity of nickel sites by modifying the electronic configuration and increasing covalency [59,60]. Ultimately, the cooperative interaction between the $Ni^{2+}/Ni^{3+}/Ni^{4+}$ and Fe^{2+}/Fe^{3+} redox couples benefits in maintaining an electronic configuration with e_g occupancy close to one, a state consistently linked to the supreme OER activity, but in some cases, it decreases long-term operation due to preferential dissolution.

The outstanding initial activity of NiFe-based oxygen evolution electrocatalysts is often compromised during prolonged operation at industrially relevant current densities (>100 mA cm^{-2}). Understanding the fundamental degradation pathways is essential for designing durable anodes. At highly oxidative OER potentials, the structural iron atoms oxidize and dissolve into the electrolyte. Under sustained, high-voltage OER conditions (often exceeding 500 mV overpotential), iron is highly prone to dissolving and leaching out of the catalyst lattice. This loss changes the optimal Ni:Fe ratio, steadily degrading catalytic activity over time. Also, at the anodic polarization, the catalyst surface undergoes continuous restructuring. Amorphous or nanocrystalline NiFe oxides gradually transform into surface-layered (oxy)hydroxide phases, accompanied by oxidation of Ni^{2+} to Ni^{3+} (and occasionally Ni^{4+}). This "electrochemical annealing" initially increases the number of active sites, but, over extended periods, leads to irreversible phase segregation. For instance, γ-Ni(Fe)OOH may convert to less active β-Ni(Fe)OOH, or the spinel structure may separate into NiO-rich and Fe_2O_3-rich domains [61,62]. Such transformations reduce the density of Ni–Fe pairs that are crucial for high OER activity. Nickel–iron LDHs are amongst the most favorable alkaline OER materials due to their earth-abundant and extraordinary activity [63,64]. Nevertheless, neither material fully overcomes the stability challenges associated with long-term operation. For instance, NiFe-LDHs undergo structural degradation as their layered morphology collapses into inactive species, decreasing the number of active sites and diminishing performance [62,65]. These catalysts experience permanent surface phase transitions between γ-Ni(Fe)OOH and β-Ni(Fe)OOH, with conflicting reports on directionality. While such transitions lead to further activity loss, the β-Ni(Fe)OOH phase is widely considered to offer higher operational stability [63,66–68]. Additionally, the leaching of Ni and Fe in alkaline solutions contributes to degradation, especially at higher currents [64,65].

Similar problems affect electrodeposited NiFe catalysts. The electrodeposition route often produces films with poor mechanical integrity, making them prone to cracking or delamination in OER environments [69,70]. Additionally, repeated surface phase transformations convert the active NiFe (oxy)hydroxide phases into inactive oxides, thereby reducing catalytic efficacy [69,70]. Extended tests similarly reveal activity loss in various electrodeposited NiFe catalysts, showing their limited durability in alkaline media [69].

Scanning electron microscopy (SEM) studies reveal that many NiFe catalysts prepared by electrodeposition or co-precipitation undergo severe morphological changes. The initially compact or nanosheet-like structure transforms into a highly porous, swollen layer that eventually detaches from the substrate. This phenomenon is attributed to deep hydration, vigorous oxygen bubble evolution, and internal stresses generated by oxygen vacancy formation [55].

The stability of NiFe catalysts is highly sensitive to the electrolyte environment. One of the most critical stability challenges is the selective dissolution of iron from NiFe catalysts. Iron dissolution from NiFe OER catalysts is heavily influenced by the interplay of electrolyte alkalinity, applied anodic potential, and the catalyst's structural defects. In alkaline electrolytes, Fe^{3+} (or Fe^{2+}) is released into the solution, especially at elevated temperatures (e.g., 60–80 °C) [55] and in concentrated KOH (5–10 M) [60]. The dissolution of iron ferrates involves the incongruent dissolution of iron-rich LDHs into water or alkaline environments, which converts or oxidizes the liberated framework iron into iron(VI), as soluble FeO_4^{2-} or iron(III) oxyhydroxides. A simplified dissolution reaction is [71,72]:

$$FeOOH + H_2O \rightarrow Fe(OH)_3(aq) + e^- \quad (17)$$

$$Fe + 8OH^- \rightarrow FeO_4^{2-} + 4H_2O + 6e^- \quad (18)$$

And it includes the formation of FeOOH and $Fe(OH)_2$ as reaction intermediates. It is also supposed that the reaction between FeOOH and $Fe(OH)_2$ produces Fe_3O_4, which can act as a barrier against additional iron dissolution and avoid the formation of ferrate, but it can also decrease OER activity. It should also be mentioned that the formed, usually colloidal, $Fe(OH)_3$ can be incorporated into the membrane, decreasing conductivity and increasing operational voltage.

The loss (corrosion) of iron reduces the Fe/Ni ratio at the surface, diminishes the synergistic Fe–Ni interaction, and increases the charge transfer resistance. Tyndall et al. [35] demonstrated that the rapid decline in activity of NiFe LDH's immediately after the startup of an alkaline cell is attributed primarily to electrochemically driven compositional degradation at active sites. Post-OER characterization using EDX, XPS, and STEM-EELS (Scanning Transmission Electron Microscopy coupled with Electron Energy-Loss Spectroscopy) reveals notable leaching of Fe compared to Ni, particularly from highly active edge sites. Additionally, post-cycle analysis identifies the formation of a ferrihydrite byproduct originating from the leached Fe. Density functional theory calculations elucidate the thermodynamic driving force behind Fe corrosion and propose a dissolution path including the elimination of $[FeO_4]^{2-}$ under OER-relevant potentials. Chronopotentiometric measurements typically show a gradual rise in overpotential over time, reflecting continuous iron depletion [73]. This effect is particularly pronounced under industrial conditions with frequent load cycling. Absorption of atmospheric CO_2 leads to carbonate formation, which can block active sites and induce the formation of passive carbonate layers, causing gradual current decay. Elevated temperature enhances OER kinetics but drastically accelerates iron leaching and phase transformation rates. While the initial overpotentials may drop, the long-term stability window narrows [55]. An optimum temperature (typically 60–80 °C) is often sought for a practical electrolyzer. Long-term OER stability remains a major hurdle, and a refined understanding of catalytic mechanisms is key to overcoming it. As highlighted in this review, surface reconstruction can cause early-stage transient dissolution, while the lattice oxygen mechanism, though beneficial for activity, may compromise structural stability. The less-studied dissolution–redeposition effect can both drive reconstruction/phase segregation and enable dynamic stability. Ultimately, practical application demands further investigation into catalyst–electrolyzer interactions to achieve durable electrolysis [22].

Scaling up NiFe-LDH catalysts for industrial water electrolysis presents several major obstructions. While they perform exceptionally well in small lab-scale batches, commercializing them is hindered. Scaling up hydrothermal synthesis for NiFe-LDH catalysts is hindered by the high energy costs of pressurized autoclaves, safety risks at large volumes, and severe reactor corrosion. The process often results in poor batch-to-batch reproducibil-

ity, particle agglomeration, and destruction of pristine layered structures, complicating mass production for industrial water splitting [74]. To avoid these hydrothermal disadvantages, researchers are successfully pivoting to substitute methods, like electrodeposition or sol–gel processes. These methods allow for direct, room temperature growth of NiFe-LDH onto conductive substrates without the need for high-pressure autoclaves. But these methods produces low adherent coatings, as mentioned before.

Last but not least is the behavior of the NiFe catalyst support. A large number of studies used nickel foam as support, but under prolonged anodic polarization, nickel forms thick non-stoichiometric semiconductor oxides with reduced conductivity, which could have a negative effect on the interlayer conductivity, and if formed through a porous catalyst layer, they can provoke pilling of the catalytic layer from the substrate [75]. Therefore, a significant study should be performed on the degradation and corrosion of different supports for the electro-active materials and their interference due to operational conditions.

5. Diagnostic Indicators of Degradation and Guidance to Young Researchers

The huge problem in comparison of the catalytic properties of materials is the undefined procedure for the electrochemical and non-electrochemical characterization. Based on the author's experience, it should be suggested that when researchers decide to investigate OER, they should prepare a minimum of four to five samples with more or less identical structures, thickness, compositions, etc. A lot of authors, after catalyst synthesis, immediately use non-electrochemical techniques to characterize samples. It could be suggested that, first, the catalytic electrochemical behavior is investigated, and if it shows good characteristics, different techniques are used to characterize the samples. Otherwise, if the catalyst did not show good characteristics, it would be a waste of time and probably money.

The electrochemical techniques, in principle, should include cyclic voltammetry (CV), a polarization curve, and a stability test.

The electrolyte choice depends, but most of the studies use 1 M NaOH or KOH solutions. The NaOH, p.a., is usually pure, but KOH is typically supplied at purities ranging from 85% to over 99.9%. Consequently, it is important to look for impurities detailed in Safety Data Sheets (MSDS) to avoid metallic impurities that can interfere with the experiments. As a reference electrode, saturated calomel or silver chloride should be avoided, as they can contaminate the electrolyte with chloride ions due to small leaks. The best choice is the Reversible Hydrogen Electrode (RHE) that can be used in any electrolyte and offers direct reading of potentials of interest. The price is around 200 USD. As a counter-electrode, avoid Pt, as it can dissolve as traces, contaminate the electrode, and give unrealistic results; glassy carbon or graphite is a much better choice. CV experiments should be performed in an inert gas (N_2, Ar) purged electrolyte, while the polarization curve should be measured in an oxygen-saturated electrolyte.

Among others, the stability test is of crucial importance. In many papers, it can be seen that, for example, the authors investigated stability with 10 mA cm^{-2} for ~15 h and concluded that excellent stability was achieved. For the electrodeposited NiFe alloy, using chronopotentiometry with 10 mA cm^{-2} for 15 h shows a potential increase of only 20 mV, while with 100 mA cm^{-2}, it shows a potential increase of almost 150 mV [76]. During the stability test, a few characteristic responses can be seen, as shown in Figure 4a. For instance, good stability is when potentials are practically not changing over time. Sometimes, a potential decrease is an indication of the surface formation of the more active species, which accelerates OER. When potentials increase over time, but not considerably, slow surface reconstruction occurs, and probably over a prolonged time, the catalyst can become inactive. The worst case is when potential increases rapidly during a short period of

time; the catalyst is useless. Stability tests should be performed with a current density of about 100–200 mA cm^{-2} over 24 h or more, which is long enough to provoke considerable surface change and to get some information about stability. Using low current densities of 5–10 mA cm^{-2} should be avoided; it can show extraordinary stability over 100 h but can be unstable at real operational conditions. Also, in some papers, it can be seen that the stability of the electrode is with 0.5 to 1 A cm^{-2}. Under such high current, oxygen evolution is considerably fast, and oxygen bubbles are formed and detached rapidly, so the measured values of the potentials will be highly unstable and scattered. If, in the paper, under such conditions someone sees a horizontal straight line, something is wrong. Also, high current produces Joule heat, and cooling or maintaining a constant temperature of the electrolyte with a thermostat is necessary. The potential should always be corrected for the *IR* drop from the impedance measurements or using instrument software; for example, the current interrupt method. After the stability test, analysis of the electrolyte with Inductively Coupled Plasma Mass Spectrometry (ICP-MS), an analytical technique used to detect trace and ultra-trace amounts of possibly dissolved metals, is highly recommended.

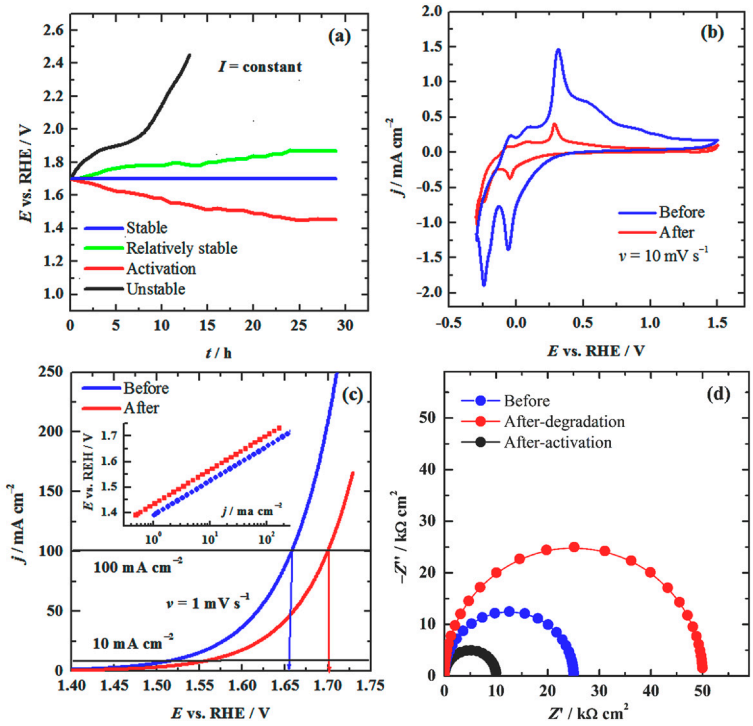

Figure 4. Simulated (**a**) stability test, (**b**) cyclic voltammograms, (**c**) polarization curves, and (**d**) electrochemical impedance spectroscopy, including a Nyquist plot, before and after the stability test.

Before the stability test, cyclic voltammetry should be used first to investigate possible redox reactions preceding oxygen evolution. The potential window should be from hydrogen to oxygen evolution potentials. It is recommended that the CV starts from negative potentials by holding potentials for 300 to 1000 s. The CV should be repeated four to five times to obtain stable behavior. The sweep rate should be 5 mV s^{-1} to 10 mV s^{-1}, which allows slow, solid-state-limited reaction peaks to be seen. Using 50 mV s^{-1} or 100 mV s^{-1} can mask some peaks. Cyclic voltammetry should be performed before and after the stability test, as shown in Figure 4b, for the electrode that does not show good performance. For a good electrode, the charge should not change significantly, but some new peaks could be seen due to structural changes of the surface layer. After the CV, polarization measurements should be performed. The potential should be held at ~1.3 V vs. RHE for ~600 s, and a slow

sweep should be used, e.g., 1 mV s^{-1} (standards recommend 0.125 mV s^{-1}, but it takes a long time). Do not use 20 mV s^{-1} or 50 1 mV s^{-1}, because electrodes cannot reach a steady state, and activity could be much better than with 1 mV s^{-1}. The polarization curve has to be recorded for current densities of 150 to 200 mA cm^{-2} at higher current densities. Due to fast oxygen bubble formation, the polarization curve will be scattered. It is recommended to record two polarization measurements to see reproducibility. After the stability test, another polarization curve should be recorded, and the results have to be similar to those before the stability test. Figure 4c shows simulated polarization curves, before and after the stability test, for a catalyst that decreases activity. If you got such a result, give up and search for a new catalyst. If the polarization curve did not show significant variations, the catalyst can be considered potentially good. Always report potentials, or overpotentials ($\eta = E - 1.23$) at 10 mA cm^{-2} and 100 mA cm^{-2}, which is standard in the literature. The best case is that the catalyst increases activity. Polarization curves have to be also shown as a Tafel plot, as a separate figure, or as an inset, as shown in Figure 4c. From the obtained Tafel slope, do not comment on the mechanism; it requires more experiments. Electrochemical impedance spectroscopy can be performed at a constant potential, determined from a polarization curve, for a current density of ~20 to 50 mA cm^{-2}, e.g., 1.4 V to 1.6 V, before and after the stability test. Figure 4d shows the characteristic Nyquist plot before the stability test, after the stability test, for the case of decreased activity (increase in Z'), and for the activated electrode (decrease in Z'). Using the appropriate equivalent electric circuit, by fitting impedance data, a lot of important parameters could be obtained.

If the catalyst shows good electrochemical characteristics, the following non-electrochemical techniques should be used to characterize the bulk and surface of the catalyst. For such characterizations, the initial sample and the sample after the stability test should be characterized.

X-ray diffraction (XRD) is a powerful, non-destructive analytical technique used by scientists to determine the atomic and molecular structure of crystalline materials. By firing X-rays at a sample and measuring the angles and intensity at which the X-rays scatter, XRD generates a unique "fingerprint" of the material's internal crystal lattice. Unfortunately, X-ray penetration depth is in the order of μm, so it is usually used for bulk characterization, and there is no need to use this technique after the stability test. After recording XRD, it is recommended that the researcher who characterizes the sample use the software usually supplied with the equipment to determine the phases of the sample.

In Figure 5 [77], the XRD of spinel $NiFe_2O_4$ is given. Typical crystal planes (hkl) are marked, corresponding to the spinel phase.

Scanning Electron Microscopy coupled with Energy-Dispersive X-ray Spectroscopy (SEM-EDS) is an analytical technique that pairs high-resolution surface imaging with elemental analysis. It works by bombarding a sample with an electron beam, which generates characteristic X-rays used to map and quantify the chemical composition of microscopic areas. The SEM coupled with EDS is a powerful tool for catalyst characterization. Depending on the X-ray energy, EDS could be near-surface characterization, for 2–7 keV, or go beyond 10 keV. With low energy, the penetration depth is limited to 100–300 nm, while it is at higher energy for μm. Penetration depth is usually given in the instrument's manual. By recording the EDS with different X-ray energies through the sample, it is possible to determine the metal concentration through the sample. Figure 6 presents SEM and EDS at 7 keV of spinel $NiFe_2O_4$ before and after the stability test at 100 mA cm^{-2} for 24 h. From SEM, it can be seen that after the stability test, the morphology changes, and EDS shows that the Fe concentration decreases, while the Ni concentration increases, which could be an indication of iron dissolution or high-surface or near-surface reconstructions.

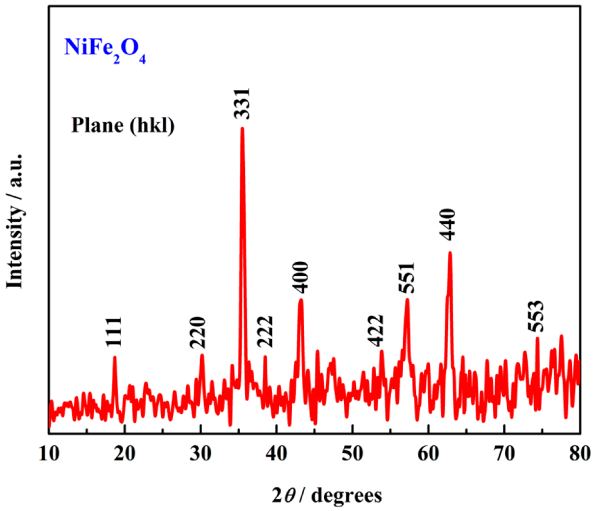

Figure 5. The XRD of spinel $NiFe_2O_4$ Adapted from Ref. [77].

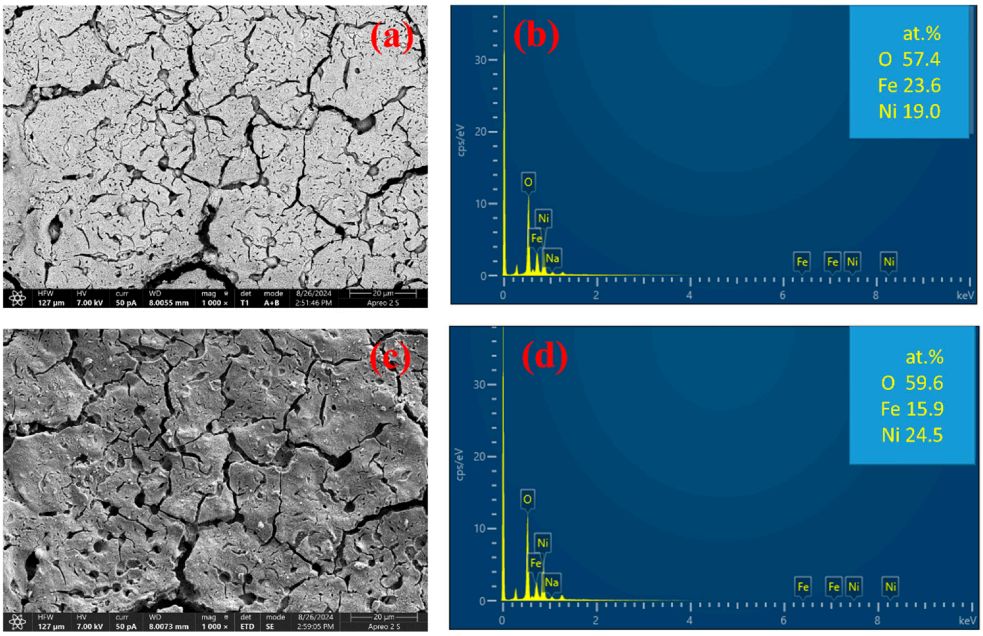

Figure 6. SEM (**a**,**c**), and EDS (**b**,**d**) at 7 keV, of spinel $NiFe_2O_4$ before and after the stability test at 100 mA cm^{-2} for 24 h. Adapted from Ref. [77].

X-ray photoelectron spectroscopy (XPS) is a powerful technique for surface catalyst characterization. The separately prepared sample without characterization after the stability test should be examined. From the XPS survey scan (0–1100 eV), the surface elemental composition of the NiFe catalyst could be determined. The high-resolution spectra shown in Figure 7 present a Ni 2p spectrum (binding energy range ~850–880 eV) that reveals the oxidation states of nickel (e.g., metallic Ni, Ni^{2+}, or Ni^{3+}) and the presence of satellite features characteristic of $Ni(OH)_2$ or NiO. The Fe 2p spectrum (~705–730 eV) indicates the dominant iron species (typically Fe^{3+} oxide/hydroxide) and possible Fe^{2+} contributions. The O 1s spectrum (~528–535 eV) distinguishes between lattice oxygen (M–O), hydroxyl groups (M–OH), and adsorbed water [78]. By fitting the spectra with appropriate software, the relative amounts of different chemical states and the surface enrichment of Fe or Ni can be quantified.

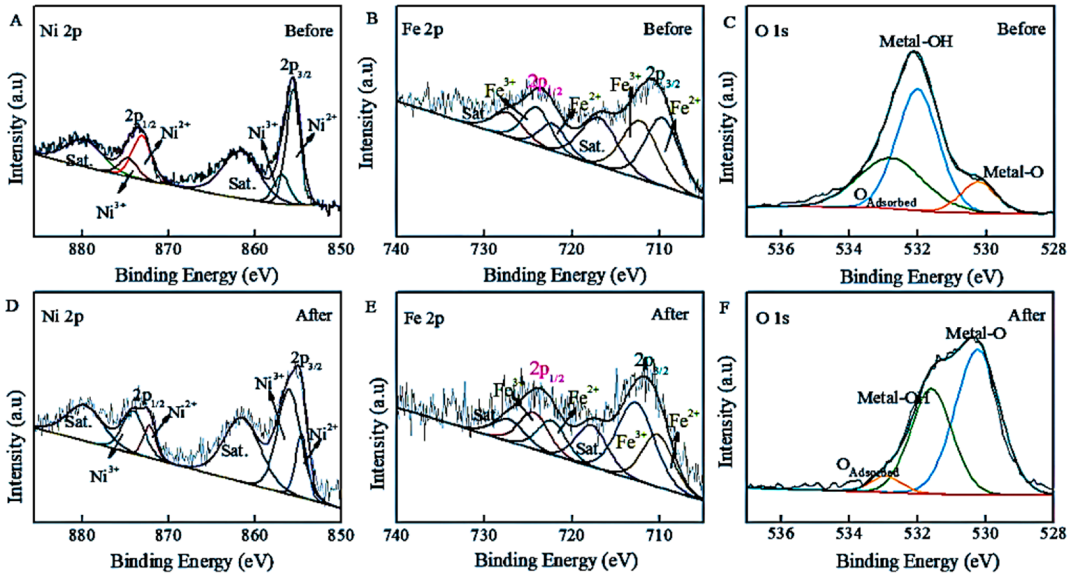

Figure 7. (**A**) XPS peaks before and after OER of the FeOOH/NiFe-LDH sample; (**A**,**D**) Ni 2p; (**B**,**E**) Fe 2p; (**C**,**F**) O1s. Adapted from Ref. [78].

This "recommendation" is only one of the possibilities for testing the OER catalyst and should be considered as guidance, not a rule.

6. Outlook and Perspective

Green hydrogen is one of the ultimate goals of energy transitions. The simplest way for production is water electrolysis. Several technologies of water electrolysis exist that are in operation or under development, including the following: alkaline water electrolysis (AWE); proton exchange membrane electrolysis (PEME); solid oxide electrolysis cells (SOEC); and anion exchange membrane electrolysis (AEME). But all of them suffer from different disadvantages. Even old alkaline water electrolysis (AWE) is still the dominant technology, but due to the high oxygen evolution overpotentials, the specific energy consumption is very high, making green hydrogen steel too expensive for broader applications. Following the great success in the research of NiFe catalysts for the oxygen evolution reaction in laboratory conditions, nickel, especially Raney nickel, as a highly porous, catalytically active form of nickel, and stainless steel electrodes continue to serve as industrial benchmarks for alkaline water electrolysis [79]. Realization of the long-term stability of OER is a serious challenge, and a more comprehensive understanding of NiFe catalytic mechanisms is required to reach this goal [22]. Also, the stability test with 5–10 mA cm^{-2} should be avoided because such investigations usually give false results of the catalyst stability. The impressive catalytic activity of nickel–iron (NiFe) (oxy)hydroxides for the oxygen evolution reaction (OER) is consistently undermined by their limited operational stability. The predominant source of this instability is the selective and continuous leaching of iron from the catalyst lattice under harsh alkaline conditions, which not only reduces the Fe/Ni ratio but also causes irreversible structural collapse of the active layered double hydroxide (LDH) architecture [35,37]. This loss of the critical Fe sites weakens the synergistic Ni–O–Fe motif and leads to a progressive increase in the overpotential and charge transfer resistance. To address this fundamental challenge, doping with specific transition metals has emerged as a highly effective strategy to electronically and structurally fortify the NiFe framework. Doping with different transition metals (e.g., Co, Mn, Mo, Ag, Cu, etc.) strengthens the NiFe framework and improves resistance to phase deviations and metal leaching [80,81]. Each dopant offers a distinct stabilization mechanism that enhances both activity and durability. Molybdenum (Mo), as a high-valence electron donor, significantly elevates the valence

states of both Ni and Fe, while shifting the d-band center of the metal active sites, which improves electrical conductivity and overall OER kinetics [82,83]. Cobalt (Co) dopants are particularly potent, as they facilitate a unique "dynamic ferrous iron regeneration" pathway that chemically restores leached Fe^{2+} species into the catalyst layer, a process that has enabled a NiFeCo LDH to maintain stable water oxidation for over 120 h [84]. Copper (Cu) functions as an efficient "electron donor," optimizing the adsorption-free energy of key OER intermediates, like *OOH, thereby synergistically boosting the intrinsic activity and stability of the resulting trimetallic NiFeCu LDH structure [85]. Silver (Ag), though less common, has proven effective by tailoring the atomically local electric field around NiFe active sites, enhancing oxygen intermediate adsorption [86]. By tackling the root cause of iron dissolution through these tailored electronic and chemical doping strategies, NiFe-based catalysts are rapidly evolving into robust and durable anodes, moving them ever closer to the long-term stability demands of industrial alkaline water electrolysis. Also, incorporating NiFe LDHs and electrodeposited NiFe layers into a conductive medium provides mechanical reinforcement and improves electron transport, thereby enhancing durability [87]. Applying protective coatings helps mitigate dissolution and suppress surface alterations [69,70]. Generally, these approaches considerably enhance the stability and working lifespan of NiFe LDH and electrodeposited NiFe OER catalysts in alkaline environments, carrying them more rapidly to application in large-scale alkaline water electrolysis. Mitigating these degradation pathways requires a holistic approach combining structural stabilization (e.g., spinel frameworks), electronic regulation, and electrolyte engineering.

Also, we proposed one of the possible experimental guidelines for testing the stability of the oxygen evolution catalyst.

With a thorough mechanistic understanding of the OER, the ultimate goal is to translate OER catalysts into practical applications. However, bridging the gap between laboratory-scale performance and real-world, large-scale operation requires closer attention to the reaction environments in which these catalysts operate, factors that are often oversimplified or overlooked in fundamental studies.

Scaling up NiFe-LDH catalysts, or some new catalyst based on NiFe oxides, for industrial water electrolysis presents the biggest major obstacles. Scaling up the hydrothermal synthesis for NiFe-LDH catalysts is overly involved by the high energy costs of pressurized autoclaves, safety risks at large volumes, and severe reactor corrosion. To avoid these hydrothermal drawbacks, researchers are successfully pivoting to substitute methods, like electrodeposition or sol–gel processes. These approaches allow for thorough, room-temperature growth of NiFe-LDH onto conductive substrates. But these methods produce low-adhesion coatings, as mentioned before.

A large number of studies cast off nickel foam as support, but under continued anodic polarization, nickel foam forms thick oxides with reduced conductivity, which could have an undesirable effect on the interlayer conductivity and could provoke pilling of the catalytic coating from the Ni-foam substrate [75]. Therefore, a significant study should be performed on the degradation and corrosion of support for electro-active materials. Pilot cell testing, which is crucial for determining the behavior of the electrolyzer, should be included in further research.

The main conclusion is that the search for a scalable and durable NiFe electrocatalyst for an oxygen evolution reaction in alkaline water electrolysis still presents a great incentive for further research.

Author Contributions: Conceptualization, B.N.G. and A.S.P.; methodology, B.N.G. and A.S.P.; writing—original draft preparation, B.N.G. and A.S.P.; writing—review and editing, B.N.G. and

A.S.P.; visualization, B.N.G. and A.S.P.; funding acquisition, B.N.G. All authors have read and agreed to the published version of the manuscript.

Funding: The support is provided by the Ministry of Education, Science and Technological Development of the Republic of Serbia, Contract No. 451-03-34/2026-03/200135.

Data Availability Statement: The original contributions presented in this study are included in the article. Further inquiries can be directed to the corresponding author.

Conflicts of Interest: The funders had no role in the design of the study; in the collection, analyses, or interpretation of data; in the writing of the manuscript; or in the decision to publish the results.

References

1. Holechek, J.L.; Geli, H.M.E.; Sawalhah, M.N.; Valdez, R. A Global Assessment: Can renewable Energy Replace Fossil Fuels by 2050? *Sustainability* **2022**, *14*, 4792. [CrossRef]
2. World Meteorological Organization (WMO). Record Carbon Emissions Highlight Urgency of Global Greenhouse Gas Watch. Available online: https://wmo.int/media/news/record-carbon-emissions-highlight-urgency-of-global-greenhouse-gas-watch (accessed on 29 May 2026).
3. Elazab, M.A.; Elgohr, A.T.; Bassyouni, M.; Kabeel, A.E.; Attia, M.E.H.; Elshaarawy, M.K.; Hamed, A.K.; Alzahrani, H.A.H. Green Hydrogen: Unleashing the Potential for Sustainable Energy Generation. *Results Eng.* **2025**, *27*, 106031. [CrossRef]
4. Nnabuife, S.G.; Darko, C.K.; Obiako, P.C.; Kuang, B.; Sun, X.; Jenkins, K. A Comparative Analysis of Different Hydrogen Production Methods and Their Environmental Impact. *Clean Technol.* **2023**, *5*, 1344–1380. [CrossRef]
5. Blumberg, T.; Morosuk, T.; Tsatsaronis, G. A Comparative Exergoeconomic Evaluation of the Synthesis Routes for Methanol Production from Natural Gas. *Appl. Sci.* **2017**, *7*, 1213. [CrossRef]
6. Franco, A.; Giovannini, C. Recent and Future Advances in Water Electrolysis for Green Hydrogen Generation: Critical Analysis and Perspectives. *Sustainability* **2023**, *15*, 16917. [CrossRef]
7. Tüysüz, H. Alkaline Water Electrolysis for Green Hydrogen Production. *Acc. Chem. Res.* **2024**, *57*, 558–567. [CrossRef] [PubMed]
8. Anand, C.; Chandraja, B.; Nithiya, P.; Akshaya, M.; Tamizhdurai, P.; Shoba, G.; Subramani, A.; Kumaran, R.; Yadav, K.K.; Gacem, A.; et al. Green hydrogen for a sustainable future: A review of production methods, innovations, and applications. *Int. J. Hydrogen Energy* **2025**, *111*, 319–341. [CrossRef]
9. Bhandari, R.; Adhikari, N. A comprehensive review on the role of hydrogen in renewable energy systems. *Int. J. Hydrogen Energy* **2024**, *82*, 923–951. [CrossRef]
10. Zhu, Y.; Keoleian, G.A.; Cooper, D.R. The role of hydrogen in decarbonizing U.S. industry: A review. *Renew. Sustain. Energy Rev.* **2025**, *214*, 115392. [CrossRef]
11. Bhuiyan, M.M.H.; Siddique, Z. Hydrogen as an alternative fuel: A comprehensive review of challenges and opportunities in production, storage, and transportation. *Int. J. Hydrogen Energy* **2025**, *102*, 1026–1044. [CrossRef]
12. Şahin, M.E. An Overview of Different Water Electrolyzer Types for Hydrogen Production. *Energies* **2024**, *17*, 4944. [CrossRef]
13. Chatenet, M.; Pollet, B.G.; Dekel, D.R.; Dionigi, F.; Deseure, J.; Millet, P.; Braatz, R.D.; Bazant, M.Z.; Eikerling, M.; Staffell, I.; et al. Water electrolysis: From textbook knowledge to the latest scientific strategies and industrial developments. *Chem. Soc. Rev.* **2022**, *51*, 4583–4762. [CrossRef] [PubMed]
14. IRENA. Green Hydrogen Cost Reduction: Scaling up Electrolysers to Meet the 1.5 °C Climate Goal, International Renewable Energy Agency, Abu Dhabi. 2020. Available online: https://www.irena.org/-/media/Files/IRENA/Agency/Publication/2020/Dec/IRENA_Green_hydrogen_cost_2020.pdf (accessed on 29 May 2026).
15. Li, Y.-F.; Li, J.-L.; Liu, Z.-P. Structure and catalysis of NiOOH: Recent advances on atomic simulation. *J. Phys. Chem. C* **2021**, *125*, 27033–27045. [CrossRef]
16. Karmakar, A.; Satheesan, A.K.; Kundu, S. Why and when does lattice oxygen participate in oxygen evolution? *Chem. Sci.* **2026**, *17*, 9327–9343. [CrossRef] [PubMed]
17. Ren, X.; Zhai, Y.; Yang, N.; Wang, B.; Liu, S. Lattice oxygen redox mechanisms in the alkaline oxygen evolution reaction. *Adv. Funct. Mater.* **2024**, *34*, 2401610. [CrossRef]
18. Xin, S.; Tang, Y.; Jia, B.; Zhang, Z.; Li, C.; Bao, R.; Li, C.; Yi, J.; Wang, J.; Ma, T. Coupling adsorbed evolution and lattice oxygen mechanism in Fe-Co$(OH)_2$/Fe_2O_3 heterostructure for enhanced electrochemical water oxidation. *Adv. Funct. Mater.* **2023**, *33*, 2305243. [CrossRef]
19. Yin, Z.-H.; Liu, H.; Hu, J.-S.; Wang, J.-J. The breakthrough of oxide pathway mechanism in stability and scaling relationship for water oxidation. *Natl. Sci. Rev.* **2024**, *11*, nwae362. [CrossRef] [PubMed]
20. Wang, Z.; Goddard, W.A.; Xiao, H. Potential-dependent transition of reaction mechanisms for oxygen evolution on layered double hydroxides. *Nat. Commun.* **2023**, *14*, 4228. [CrossRef] [PubMed]

21. De Araújo, J.F.; Dionigi, F.; Merzdorf, T.; Oh, H.; Strasser, P. Evidence of Mars-Van-Krevelen mechanism in the electrochemical oxygen evolution on Ni-based catalysts. *Angew. Chem. Int. Ed.* **2021**, *60*, 14981–14988. [CrossRef] [PubMed]
22. Chen, F.-Y.; Wu, Z.-Y.; Adler, Z.; Wang, H. Stability challenges of electrocatalytic oxygen evolution reaction: From mechanistic understanding to reactor design. *Joule* **2021**, *5*, 1704–1731. [CrossRef]
23. Fabbri, E.; Schmidt, T.J. Oxygen Evolution Reaction—The Enigma in water electrolysis. *ACS Catal.* **2018**, *8*, 9765–9774. [CrossRef]
24. Li, P.; Jang, H.; Zhang, J.; Tian, M.; Chen, S.; Yuan, B.; Wu, Z.; Liu, X.; Cho, J. A Metal-Free N and P-Codoped carbon nanosphere as bifunctional electrocatalyst for rechargeable Zinc-Air batteries. *ChemElectroChem* **2018**, *6*, 393–397. [CrossRef]
25. Tachikawa, T.; Beniya, A.; Shigetoh, K.; Higashi, S. Relationship Between OER Activity and Annealing Temperature of Sputter-Deposited Flat IrO_2 Thin Films. *Catal. Lett.* **2020**, *150*, 1976–1984. [CrossRef]
26. Palani, R.; Anitha, V.; Karuppiah, C.; Rajalakshmi, S.; Li, Y.-J.J.; Hung, T.-F.; Yang, C.-C. Imidazolatic-Framework Bimetal Electrocatalysts with a Mixed-Valence Surface Anchored on an rGO Matrix for Oxygen Reduction, Water Splitting, and Dye Degradation. *ACS Omega* **2021**, *6*, 16029–16042. [CrossRef] [PubMed]
27. Chen, H.; Huang, X.; Zhou, L.-J.; Li, G.-D.; Fan, M.; Zou, X. Electrospinning Synthesis of Bimetallic Nickel–Iron Oxide/Carbon Composite Nanofibers for Efficient Water Oxidation Electrocatalysis. *ChemCatChem* **2016**, *8*, 992. [CrossRef]
28. Si, S.; Hu, H.-S.; Liu, R.-J.; Xu, Z.-X.; Wang, C.-B.; Feng, Y.-Y. Co–NiFe layered double hydroxide nanosheets as an efficient electrocatalyst for the electrochemical evolution of oxygen. *Int. J. Hydrogen Energy* **2020**, *45*, 9368–9379. [CrossRef]
29. Corrigan, D.A. The catalysis of the oxygen evolution reaction by iron impurities in thin-film nickel oxide electrodes. *J. Electrochem. Soc.* **1987**, *134*, 377–384. [CrossRef]
30. Trotochaud, L.; Young, S.L.; Ranney, J.K.; Boettcher, S.W. Nickel–iron oxyhydroxide oxygen-evolution electrocatalysts: The role of intentional and incidental iron incorporation. *J. Am. Chem. Soc.* **2014**, *136*, 6744–6753. [CrossRef] [PubMed]
31. Gong, M.; Li, Y.; Wang, H.; Liang, Y.; Wu, J.Z.; Zhou, J.; Wang, J.; Regier, T.; Wei, F.; Dai, H. An advanced Ni–Fe layered double hydroxide electrocatalyst for water oxidation. *J. Am. Chem. Soc.* **2013**, *135*, 8452–8455. [CrossRef] [PubMed]
32. Mohammed-Ibrahim, J. A review on NiFe-based electrocatalysts for efficient alkaline oxygen evolution reaction. *J. Power Sources* **2020**, *448*, 227375. [CrossRef]
33. Kulkarni, S.S.; Khande, G.L.; Gunjakar, J.L.; Koli, V.B. Advances in Layered Double Hydroxide (LDH)-Based Materials for Electrocatalytic Nitrogen Reduction to Ammonia: A Comprehensive Review. *Nitrogen* **2025**, *6*, 106. [CrossRef]
34. Guo, D.; Chi, J.; Yu, H.; Jiang, G.; Shao, Z. Self-Supporting NiFe Layered Double Hydroxide "Nanoflower" Cluster Anode Electrode for an Efficient Alkaline Anion Exchange Membrane Water Electrolyzer. *Energies* **2022**, *15*, 4645. [CrossRef]
35. Tyndall, D.; Craig, M.J.; Gannon, L.; McGuinness, C.; McEvoy, N.; Roy, A.; García Melchor, M.; Browne, M.P.; Nicolosi, V. Demonstrating the source of inherent instability in NiFe LDH based OER electrocatalysts. *J. Mater. Chem. A* **2023**, *11*, 4067–4077. [CrossRef] [PubMed]
36. Li, Z.; Shao, M.; An, H.; Wang, Z.; Xu, S.; Wei, M.; Evans, D.G.; Duan, X. Fast electrosynthesis of Fe containing layered double hydroxide arrays toward highly efficient electrocatalytic oxidation reactions. *Chem. Sci.* **2015**, *6*, 6624–6631. [CrossRef] [PubMed]
37. Liu, Q.; Wang, Y.; Lu, X. Construction of NiFe Layered Double Hydroxides Arrays as Robust Electrocatalyst for Oxygen Evolution Reaction. *Catalysts* **2023**, *13*, 586. [CrossRef]
38. Li, T.; Liu, W.; Xin, H.; Sha, Q.; Xu, H.; Kuang, Y.; Sun, X. Large-Scale and Simple Synthesis of $NiFe(OH)_x$ Electrode Derived from Raney Ni Precursor for Efficient Alkaline Water Electrolyzer. *Catalysts* **2024**, *14*, 296. [CrossRef]
39. Li, G.; Zhang, J.; Li, L.; Yuan, C.; Weng, T.-C. Boosting the Electrocatalytic Activity of Nickel-Iron Layered Double Hydroxide for the Oxygen Evolution Reaction by Terephthalic Acid. *Catalysts* **2022**, *12*, 258. [CrossRef]
40. Zhang, Z.; Zhou, D.; Bao, X.; Yu, H.; Huang, B. Thermal decomposition behavior of nickel-iron hydrotalcite and its electrocatalytic properties of oxygen reduction and oxygen evolution reactions. *Int. J. Hydrogen Energy* **2018**, *43*, 20734–20738. [CrossRef]
41. Quiroz, S.G.; Cartagena, S.; Calderón, J.A. Enhancement of oxygen evolution performance of water splitting at high current density by novel electrodeposited NiFe-LDH coatings. *Electrochim. Acta* **2025**, *528*, 146332. [CrossRef]
42. Lu, X.; Zhao, C. Electrodeposition of hierarchically structured three-dimensional nickel–iron electrodes for efficient oxygen evolution at high current densities. *Nat. Commun.* **2015**, *6*, 6616. [CrossRef] [PubMed]
43. Swierk, J.R.; Klaus, S.; Trotochaud, L.; Bell, A.T.; Tilley, T.D. Electrochemical study of the energetics of the oxygen evolution reaction at nickel iron (oxy)hydroxide catalysts. *J. Phys. Chem. C* **2015**, *119*, 19022–19029. [CrossRef]
44. Wu, X.; Du, Y.; An, X.; Xie, X. Fabrication of NiFe layered double hydroxides using urea hydrolysis—Control of interlayer anion and investigation on their catalytic performance. *Catal. Commun.* **2014**, *50*, 44–48. [CrossRef]
45. Zuber, A.; Oikonomou, I.M.; Gannon, L.; Chunin, I.; Reith, L.; Can, B.; Lounasvuori, M.; Schultz, T.; Koch, N.; McGuinness, C.; et al. Effect of the precursor metal salt on the oxygen evolution reaction for NiFe oxide materials. *ChemElectroChem* **2024**, *11*, e202400151. [CrossRef]
46. Hou, C.; Cui, Z.; Zhang, S.; Yang, W.; Gao, H.; Luo, X. Rapid large scale synthesis of ultrathin NiFe LDH nanosheets with tunable structures as robust oxygen evolution electrocatalysts. *RSC Adv.* **2021**, *11*, 37624–37630. [CrossRef] [PubMed]

47. Iwasaki, T.; Yoshii, H.; Nakamura, H.; Watano, S. Simple and rapid synthesis of Ni–Fe layered double hydroxide by a new mechanochemical method. *Appl. Clay Sci.* **2012**, *58*, 120–124. [CrossRef]
48. Molina-Muriel, M.; Zignani, S.C.; Goberna-Ferrón, S.; Ribera, A.; Aricò, A.S.; García, H. Efficient NiFe-Layered double hydroxide electrocatalyst synthesized via a solvent-free mechanochemical method for oxygen evolution reaction. *ACS Omega* **2025**, *10*, 22671–22678. [CrossRef] [PubMed]
49. Del Rosario, J.A.D.; Li, G.; Labata, M.F.M.; Ocon, J.D.; Chuang, P.-Y.A. Unravelling the roles of alkali-metal cations for the enhanced oxygen evolution reaction in alkaline media. *Appl. Catal. B Environ.* **2021**, *288*, 119981. [CrossRef]
50. Garcia, A.C.; Touzalin, T.; Nieuwland, C.; Perini, N.; Koper, M.T.M. Enhancement of oxygen evolution activity of nickel oxyhydroxide by electrolyte alkali cations. *Angew. Chem. Int. Ed.* **2019**, *58*, 12999–13003. [CrossRef] [PubMed]
51. Zhuang, D.; Riera, M.; Zhou, R.; Deary, A.; Paesani, F. Hydration structure of Na^+ and K^+ ions in solution predicted by data-driven many-body potentials. *J. Phys. Chem. B* **2022**, *126*, 9349–9360. [CrossRef] [PubMed]
52. Li, D.; Park, E.J.; Zhu, W.; Shi, Q.; Zhou, Y.; Tian, H.; Lin, Y.; Serov, A.; Zulevi, B.; Baca, E.D.; et al. Highly quaternized polystyrene ionomers for high performance anion exchange membrane water electrolysers. *Nat. Energy* **2020**, *5*, 378–385. [CrossRef]
53. Kubo, N.M.; Ketter, F.; Palkovits, S.; Palkovits, R. Nickel and Commercially Available Nickel-Containing Alloys as Electrodes for the Electrochemical Oxygen Evolution. *ChemElectroChem* **2024**, *11*, e202300460. [CrossRef]
54. Luo, Y.; He, Y.; Li, J.; Wei, S.; Chen, L. Reinforced lattice oxygen mechanism of NiFe-LDH@Fe_2O_3@NF by optimizing the adsorption of oxygen intermediates for efficient water electrolysis. *J. Environ. Chem. Eng.* **2025**, *13*, 115497. [CrossRef]
55. Han, Y.; Wang, J.; Liu, Y.; Li, T.; Wang, T.; Li, X.; Ye, X.; Li, G.; Li, J.; Hu, W.; et al. Stability challenges and opportunities of NiFe-based electrocatalysts for oxygen evolution reaction in alkaline media. *Carbon Neutraliz.* **2024**, *3*, 172–198. [CrossRef]
56. Chen, X.; Huang, C.; Liu, J.; Xiang, Q.; Zhang, L.; Huang, X.; Li, L.; Wei, Z. Dynamic stability of OER electrocatalysts in water electrolyzers: Multiscale deactivation mechanisms and regulation strategies. *Chem. Sci.* **2026**. [CrossRef] [PubMed]
57. Li, L.; Bai, L.; She, S.; Chen, G.; Huang, H. Mixed ionic conductor brings extra gain in oxygen-evolving activity of NiFe hydroxide electrocatalyst at practical working temperature. *Appl. Catal. B Environ. Energy* **2025**, *371*, 125271. [CrossRef]
58. Pascuzzi, M.E.C.; Man, A.J.W.; Goryachev, A.; Hofmann, J.P.; Hensen, E.J.M. Investigation of the stability of NiFe-(oxy)hydroxide anodes in alkaline water electrolysis under industrially relevant conditions. *Catal. Sci. Technol.* **2020**, *10*, 5593–5601. [CrossRef]
59. Goldsmith, Z.K.; Young, S.L.; Ranney, J.K.; Boettcher, S.W. Characterization of NiFe Oxyhydroxide Electrocatalysts by Integrated Electronic Structure Calculations and Spectroelectrochemistry. *Proc. Natl. Acad. Sci. USA* **2017**, *114*, 3050–3055. [CrossRef] [PubMed]
60. El Boumlasy, S.; Pascale, M.; De Luca, O.; Caruso, T.; Mirabella, S.; Terrasi, A.; Aricò, A.S.; Ruffino, F. Highly efficient and stable NiFe oxide-based electrocatalysts for oxygen evolution in alkaline and saline solutions. *Appl. Surf. Sci. Adv.* **2025**, *28*, 100809. [CrossRef]
61. Lin, Z.; Bu, P.; Xiao, Y.; Gao, Q.; Diao, P. β- and γ-NiFeOOH electrocatalysts for an efficient oxygen evolution reaction: An electrochemical activation energy aspect. *J. Mater. Chem. A* **2022**, *10*, 20847–20855. [CrossRef]
62. Feng, Z.; Wang, P.; Cheng, Y.; Mo, Y.; Luo, X.; Liu, P.; Guo, R.; Liu, X. Recent progress on $NiFe_2O_4$ spinels as electrocatalysts for the oxygen evolution reaction. *J. Electroanal. Chem.* **2023**, *946*, 117703. [CrossRef]
63. He, L.; Zhou, Y.; Wang, M.; Li, S.; Lai, Y. Recent Progress on Stability of Layered Double Hydroxide-Based Catalysts for Oxygen Evolution Reaction. *Nanomaterials* **2024**, *14*, 1533. [CrossRef] [PubMed]
64. Iqbal, S.; Ehlers, J.C.; Hussain, I.; Zhang, K.; Chatzichristodoulou, C. Trends and industrial prospects of NiFe-layered double hydroxide for the oxygen evolution reaction. *Chem. Eng. J.* **2024**, *499*, 156219. [CrossRef]
65. Plevová, M.; Hnát, J.; Bouzek, K. Electrocatalysts for the Oxygen Evolution Reaction in Alkaline Media: A Comparative Review. *J. Power Sources* **2021**, *507*, 230072. [CrossRef]
66. Soni, A.; Maurya, S.K.; Malviya, M. Exploring electrocatalysts for oxygen evolution: A comprehensive comparative review in alkaline and acidic medium. *J. Power Sources* **2025**, *636*, 236571. [CrossRef]
67. Li, L.-F.; Li, Y.-F.; Liu, Z.-P. Oxygen Evolution Activity on NiOOH Catalysts: Four-Coordinated Ni Cation as the Active Site and the Hydroperoxide Mechanism. *ACS Catal.* **2020**, *10*, 2581–2590. [CrossRef]
68. Li, X.; Ruan, M.; Shen, Y.; Wen, M.; Li, Z.; Yin, H.; Chen, F.; Cheng, Y.; Lei, P.; Qian, L. Phase locking of NiOOH@β-Ni(Fe)OOH reconstructed simultaneously for robust oxygen evolution at high current density. *ACS Appl. Mater. Interfaces* **2025**, *17*, 44562–44572. [CrossRef] [PubMed]
69. Han, S.; Yoon, J. Strategies for Advancing Electrodeposited Co-Based Oxygen Evolution Catalysts from Alkaline to Pure-Water Conditions. *ACS Mater. Lett.* **2025**, *7*, 3128–3140. [CrossRef]
70. McCrory, C.C.L.; Jung, S.; Peters, J.C.; Jaramillo, T.F. Benchmarking heterogeneous electrocatalysts for the oxygen evolution reaction. *J. Am. Chem. Soc.* **2013**, *135*, 16977–16987. [CrossRef] [PubMed]
71. Vital, M.; Van Beek Pedersen, T.; Molander, J.; Jakobsen, R.; Tobler, D.J.; Dideriksen, K. Dissolution kinetics for the Fe(II)-Fe(III) layered double hydroxide, green rust. *Appl. Clay Sci.* **2025**, *272*, 107814. [CrossRef]

72. De Koninck, M.; Bélanger, D. The electrochemical generation of ferrate at pressed iron powder electrode: Comparison with a foil electrode. *Electrochim. Acta* **2003**, *48*, 1435–1442. [CrossRef]
73. 72Wu, Y.; Zhang, C.; Fei, Y.; Zheng, Z. The degradation mechanism of NiFe-LDH catalysts in alkaline oxygen evolution reaction at high temperature. *Mater. Lett.* **2025**, *398*, 138901. [CrossRef]
74. Wan, Z.; Ma, Z.; Yuan, H.; Liu, K.; Wang, X. Sulfur engineering on NIFE layered double hydroxide at ambient temperature for high current density oxygen evolution reaction. *ACS Appl. Energy Mater.* **2022**, *5*, 4603–4612. [CrossRef]
75. Ye, H.; Zhang, J.; Chen, Q.; Feng, C.; Quan, Z.; Zhang, G.; Fan, X.; Zhang, J.; Li, Y. Solvent-engineered crystalline-amorphous NiFe LDH electrocatalysts with industrial-grade stability for enhanced water oxidation. *J. Energy Chem.* **2025**, *111*, 650–658. [CrossRef]
76. Elsharkawy, S.; Żabiński, P. Effect of Fe/Ni ratio on electrodeposition of Ni-Fe alloys and their bifunctional catalytic performance in hydrogen and oxygen evolution reactions. *J. Power Sources* **2025**, *660*, 238516. [CrossRef]
77. Grgur, B.N. (Faculty of Technology and Metalyrgu, University of Belgrade, Karnegijeva 4, Belgrede, Serbia); Popović, A.S. (Faculty of Technology and Metalyrgu, University of Belgrade, Karnegijeva 4, Belgrede, Serbia). Unpublished work. 2025. [CrossRef]
78. Yu, J.; Fu, X.; Wang, H.; Lu, S.; Li, B. Rational construction of nano-scaled FeOOH/NiFe-LDH for efficient water splitting. *Nanomaterials* **2025**, *15*, 949. [CrossRef] [PubMed]
79. Nikolić, V.M.; Dimić-Mišić, K.M.; Maslovara, S.L.; Popović, D.P.; Gigov, M.N.; Krstić, S.S.; Kaninski, M.P.M. Advances in Alkaline Water Electrolysis—The role of in situ ionic activation in green hydrogen production. *Catalysts* **2026**, *16*, 98. [CrossRef]
80. Qiao, X.; Zhu, Q.; Hou, G.; Pang, Z.; Kang, H. Pinning effect of lattice Co enhances lattice oxygen regeneration in NiFe-LDH for oxygen evolution reaction. *J. Colloid Interface Sci.* **2025**, *699*, 138219. [CrossRef] [PubMed]
81. Xie, X.; Du, L.; Yan, L.; Park, S.; Qiu, Y.; Sokolowski, J.; Wang, W.; Shao, Y. Oxygen evolution reaction in alkaline environment: Material challenges and solutions. *Adv. Funct. Mater.* **2022**, *32*, 2110036. [CrossRef]
82. Zhang, C.; Wang, J.; Ma, H.; Wang, J.; Xu, R.; Li, G.; Yang, L.; Guo, H. Electronic structure engineering of NiFe hydroxide nanosheets via ion doping for efficient OER electrocatalysis. *Chem. Eng. J.* **2024**, *499*, 156430. [CrossRef]
83. Qu, J.; Dong, Y.; Zhang, T.; Zhao, C.; Wei, L.; Guan, X. Impact of bimetallic synergies on Mo-doping NiFeOOH: Insights into enhanced OER activity and reconstructed electronic structure. *Front. Energy* **2024**, *18*, 850–862. [CrossRef]
84. Assavachin, S.; Ittisanronnachai, S.; Atithep, T.; Chitterisin, N.; Sawangphruk, M. Dynamic ferrous iron regeneration enables stabilization of NiFeCo layered double hydroxide for enhanced alkaline water oxidation. *J. Power Sources* **2025**, *650*, 237494. [CrossRef]
85. Li, J.; Wei, Y.; Zou, L.; Liu, Y.; Li, S.; Luo, Y. Cu dual-site doping: Synergistic enhancement of OER activity through LDH and nickel foam interface engineering. *New J. Chem.* **2025**, *49*, 17577–17587. [CrossRef]
86. Zhang, X.; Tong, L.; Shi, X.; Li, Z.; Xiao, Z.; Liu, Y.; Zhang, T.; Lin, S. Tailoring atomically local electric field of NiFe layered double hydroxides with Ag dopants to boost oxygen evolution kinetics. *J. Colloid Interface Sci.* **2024**, *668*, 502–511. [CrossRef] [PubMed]
87. Silva, A.S.-D.; Hartert, A.; Oestreicher, V.; Romero, J.; Jaramillo-Hernández, C.; Muris, L.J.J.; Thorez, G.; Vieira, B.J.C.; Ducourthial, G.; Fiocco, A.; et al. Scalable synthesis of NiFe-layered double hydroxide for efficient anion exchange membrane electrolysis. *Nat. Commun.* **2025**, *16*, 6138. [CrossRef] [PubMed]